Diffusion of water submonolayers on hydrophilic surfaces

Jae Hyun Park and N. R. Aluru[a)]
Department of Mechanical Science and Engineering, Beckman Institute for Advanced Science and Technology, University of Illinois at Urbana-Champaign, Urbana, Illinois 61801, USA

(Received 4 September 2008; accepted 27 November 2008; published online 22 December 2008)

In this letter, we investigate using molecular dynamics simulations the diffusion of water submonolayers on hydrophilic surfaces. In contrast to a strong hydrophilic Ag surface, on a weak hydrophilic Pb surface, the diffusion coefficient is remarkably enhanced at a critical surface coverage and a Λ-shape anomaly with surface coverage is observed, i.e., the diffusion coefficient increases with the increase in surface coverage until a critical surface coverage, beyond which the diffusion coefficient decreases. We explain the anomalous diffusion of water on hydrophilic surfaces by a detailed understanding of molecular cavities and monolayer tail contributing to three-dimensional hydrogen bonding. © *2008 American Institute of Physics*.
[DOI: 10.1063/1.3054640]

Transport of liquid submonolayers on solid substrates has gained significant attention recently because of applications in nanolithography, nanoprinting, wetting/dewetting of nanopatterned surfaces, etc.[1] Diffusion of submonolayer liquids can be markedly different from diffusion of bulk liquids or diffusion of thick (thicknesses of the order of several nanometers) liquid films on surfaces. For example, diffusion of *n*-alkane and long polyethylene glycol submonolayers exhibits nonmonotonic dependence on the surface coverage, i.e., the surface diffusion increases with increasing surface concentration and then decreases abruptly.[2] Even though water is considered to be the *most fundamental and basic working fluid*, diffusion of water submonolayers on solid substrates has not been investigated so far.

In this letter, we use molecular dynamics simulations to investigate diffusion of water on hydrophilic surfaces when the surface coverage is less than a monolayer—also referred to as incomplete coverage. Two typical hydrophilic surfaces—namely, a Ag surface and a Pb surface—were considered. The Ag surface is considered as a strong hydrophilic surface with (6-12) Lennard-Jones parameters of $\sigma_{Ag}=0.2544$ nm and $\epsilon_{Ag}=33.2664$ kJ/mol [$\epsilon_{Ag\text{-}OW}=4.6508$ kJ/mol, where OW is the oxygen atom inextended simple point charge (SPC/E)water[3]] while the Pb surface is considered as a weak hydrophilic surface with $\sigma_{Pb}=0.3197$ nm and $\epsilon_{Pb}=22.8067$ kJ/mol.[4] For each surface, various surface coverages (denoted by Γ) ranging from $\Gamma=0.201$ mg/m^2 to $\Gamma=\Gamma_{full}=0.376$ g/m^2 for Pb surface and $\Gamma=0.201$ mg/m^2 to $\Gamma=\Gamma_{full}=0.393$ g/m^2 for Ag surface were considered. The surface coverage is measured as the ratio of the total mass of the water molecules to the surface area. Figure 1 summarizes the various cases considered for Pb surface. For Pb surface, when the surface coverage is smaller than $\Gamma=0.201$ mg/m^2, the water layer is separated completely into two parts while for the Ag surface when $\Gamma<0.322$ mg/m^2, we hardly see the transport of molecules. From the view point of density, the surface is considered to be fully covered for $\Gamma_{full}=0.376$ mg/m^2 for Pb surface and $\Gamma_{full}=0.393$ mg/m^2 for Ag surface. Beyond this coverage, a second layer starts to form (see the density plot in Fig. 1).

Simulations were performed using GROMACS 3.2.1 (Ref. 5) in an *NVT* ensemble. Both Ag and Pb surfaces have fcc structure.[6] The surface consists of three layers and the dimensions of each layer are 3.58×3.58 nm^2 (*xy*-plane) for Pb-surface and 3.50×3.50 nm^2 for Ag surface. Periodic boundary conditions were assigned along the *x* and *y* directions. All the simulations were equilibrated for 2 ns. The sampling period was 22 ns. Water was modeled as SPC/E model[3] and the interatomic interaction between solid atoms was modeled by using the Morse potential.[6] The Nosé–Hoover thermostat[7] was used to maintain the system tem-

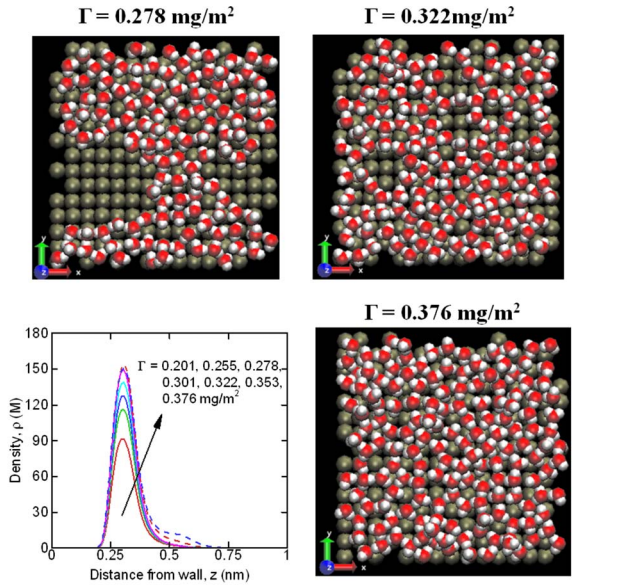

N_{Wt}	86	109	119	129	138	151	161
Γ (mg/m^2)	0.201	0.255	0.278	0.302	0.322	0.353	0.376

FIG. 1. (Color online) Molecular visualization of water submonolayers on the Pb surface and the corresponding density plots. The snapshots were rendered using VMD (Ref. 13). The table summarizes the various surface coverage conditions considered for the Pb surface. N_{Wt} is the number of waters in the system.

a)Author to whom correspondence should be addressed. Electronic mail: aluru@illinois.edu. URL: https://netfiles.uiuc.edu/aluru/www/.

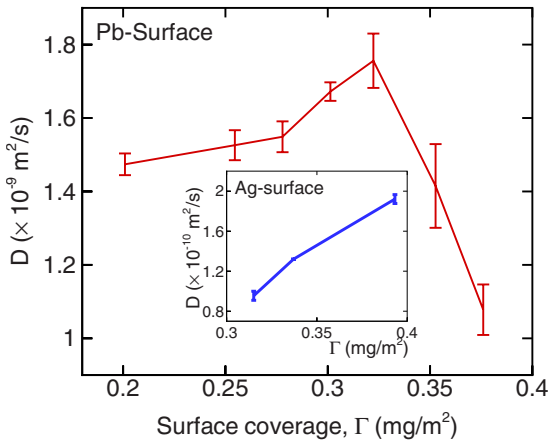

FIG. 2. (Color online) Diffusion coefficient of water on Pb and Ag surfaces for various surface coverages.

perature at 300 K. The equation of motion was integrated by using the leapfrog algorithm with a time step of 2.0 fs.

Figure 2 shows the lateral diffusion coefficient of water for various surface coverages. Diffusion perpendicular to the solid surface is negligible ($D_{\perp} \sim 10^{-12}$ m^2/s), so we do not investigate it any further in this study. Lateral diffusion coefficient was computed from the mean-squared displacement of water, $D=\lim_{t\to\infty}[\langle|\mathbf{R}_{\text{c.m.}}(t)-\mathbf{R}_{\text{c.m.}}(0)|^2\rangle/4t]$, where $\mathbf{R}_{\text{c.m.}}$ is the (x,y) position of the center of mass of the water molecule. Throughout this letter, *diffusion* coefficient refers to the *lateral diffusion* coefficient unless specified otherwise. From Fig. 2, we observe a clear difference between diffusion on strong and weak hydrophilic surfaces. As shown in Fig. 2 inset, for the strong hydrophilic Ag surface, water molecules are significantly immobilized ($D<10^{-11}$ m^2/s, data not shown in the figure) when Γ is less than 0.322 mg/m^2 because the water-surface interaction ($\epsilon_{\text{Ag-OW}}$ =4.6508 kJ/mol) is significantly stronger compared to the water-water interaction ($\epsilon_{\text{OW-OW}}$=0.6502 kJ/mol). The maximum diffusion coefficient is found to be 1.92 $(\pm 0.045)\times 10^{-10}$ m^2/s at $\Gamma=\Gamma_{\text{full}}$=0.393 mg/m^2. In contrast to the Ag surface, for the weak hydrophilic Pb surface we observe considerable diffusion with *anomalous* Λ *behavior*: the diffusion coefficient gradually increases with the decrease in surface coverage until it reaches a critical surface coverage (Γ_{crit}=0.322 mg/m^2) and then starts to decrease with a further decrease in the surface coverage (this is referred to as Λ shape[2]). The maximum diffusion coefficient at $\Gamma=\Gamma_{\text{crit}}$ is 1.76 $(\pm 0.074)\times 10^{-9}$ m^2/s, which is about 1.7 times larger than the value of D=1.08 $(\pm 0.069)\times 10^{-9}$ m^2/s at $\Gamma=\Gamma_{\text{full}}$. Since the Pb surface has a much smaller ϵ_{Pb}, diffusion becomes substantial and the interplay between water-water and water-surface interactions becomes important. If the diffusion is governed by water-surface interactions, the water-surface interaction energy should exhibit a similar trend to that of the diffusion. However, the surface-water interaction energy is found to be around −14 kJ/mol regardless of the surface coverage, which indicates that the anomalous diffusion of water on the weak hydrophilic Pb surface is primarily due to the water-water interactions while the solid surface just holds the water molecules on the surface steadily. As diffusion of water on Ag surface is insignificant, in the discussion to follow, we will focus on the weak hydrophilic Pb surface to understand the diffusion mechanism as a function of surface coverage. Hereafter, surface refers to the Pb surface unless noted otherwise.

As shown in Fig. 1, the water submonolayer has a number of depletion zones (empty regions on the surface). The depletion zones were identified by using the Hoshen–Kopelman percolation algorithm[8] and then the number and size distributions were computed. Considering that the molecular transport in dense fluids proceeds primarily by a large number of small jumps whose lengths are approximately equal to the intermolecular spacing rather than a few large ones,[9] we used 2.77 times the size of a water molecule ($d_{\text{H}_2\text{O}}$=0.2785 nm) as the criterion, v_{crit}, to differentiate between small (favorable for diffusion) and large (not very favorable for diffusion) depletion zones. If the size of the depletion zone, v, is smaller than v_{crit}, the depletion zone is referred to as molecular cavity and if the size is larger than v_{crit}, it is referred to as macroscopic void. Typically, more than 95% of the depletion zones are molecular cavities while only less than 5% are macroscopic voids.

Figure 3(a) shows the variation of the average size of the molecular cavity as a function of surface coverage Γ. For a given surface coverage, the average size of the molecular cavity is computed using the expression

$$v_{\text{avg}}^{\text{cavity}} = \int_0^{v_{\text{crit}}} v p_{\text{size}}^{\text{cavity}}(v)dv, \tag{1}$$

where $p_{\text{size}}^{\text{cavity}}(v)$ is the size distribution function of molecular cavities. Figure 3(b) shows the variation of the average number of molecular cavities per water molecule as a function of Γ. The average number of molecular cavities per water molecule is defined as

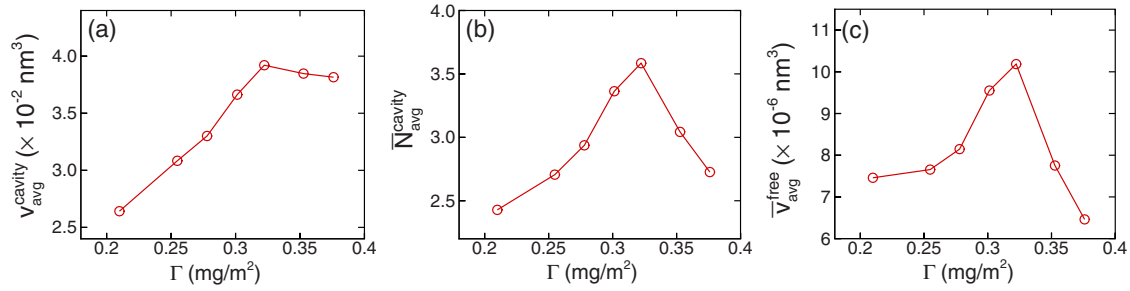

FIG. 3. (Color online) Statistics of molecular cavities for various surface coverages: (a) average size of molecular cavity; (b) average number of molecular cavities per water molecule; (c) normalized molecular free volume.

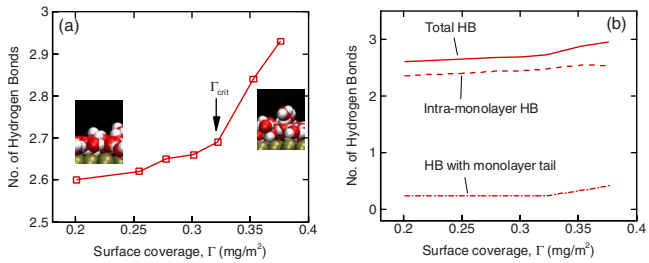

FIG. 4. (Color online) (a) Number of HBs per water molecule for various surface coverages; (b) contributions from intramonolayer HB and the HB with monolayer tail on the total HB.

$$\bar{N}_{\text{avg}}^{\text{cavity}} = \frac{1}{N_{\text{Wt}}(\Gamma)} \int_0^{N(v \leqslant v_{\text{crit}})} N p_{\text{number}}^{\text{cavity}}(N) dN, \tag{2}$$

where $N_{\text{Wt}}(\Gamma)$ is the number of water molecules which is a function of Γ, N is the number of molecular cavities, and $p_{\text{number}}^{\text{cavity}}(N)$ is the number distribution function of molecular cavities. Both the average size and number of molecular cavities per water molecule have their maxima at $\Gamma_{\text{crit}} = 0.322\ \text{mg/m}^2$, which confirms that molecular cavities play an important role in diffusion. Furthermore, in Fig. 3(c) we normalized the molecular free volume, $v_{\text{avg}}^{\text{free}} = \bar{N}_{\text{avg}}^{\text{cavity}} \times v_{\text{avg}}^{\text{cavity}}$, by the number of water molecules in the system, $N_{\text{Wt}}(\Gamma)$, as $\bar{v}_{\text{avg}}^{\text{free}} = \bar{N}_{\text{avg}}^{\text{cavity}} \times v_{\text{avg}}^{\text{cavity}} / N_{\text{Wt}}(\Gamma)$. We found that $\bar{v}_{\text{avg}}^{\text{free}}$ captures the features of diffusion (shown in Fig. 2) better than $v_{\text{avg}}^{\text{cavity}}$ or $\bar{N}_{\text{avg}}^{\text{cavity}}$ alone. Given this observation, we can assume a simple relation between the diffusion coefficient and the normalized molecular free volume:

$$D \propto \bar{v}_{\text{avg}}^{\text{free}} = \frac{v_{\text{avg}}^{\text{free}}}{N_{\text{Wt}}(\Gamma)}. \tag{3}$$

Equation (3) is quite similar to the corrected Enskog diffusion formula for a bulk hard-sphere liquid,[10] which also expresses that the diffusion coefficient is proportional to the molecular free volume and inversely proportional to the number of molecules.

We also examined the hydrogen bonding (HB) characteristics to further understand the diffusion phenomena. HB was defined using a geomeric criterion.[11] Figure 4(a) shows the number of hydrogen bonds (n_{HB}) for various surface coverages. A significant increase in n_{HB} is observed after $\Gamma_{\text{crit}} = 0.322\ \text{mg/m}^2$, where we can see the formation of the monolayer tail while the second layer has not been formed yet (see Fig. 1). When the tail is formed, as seen from the molecular visualizations in the inset of Fig. 4(a), the chance for a molecule to go on top of another molecule increases, whereas in the case of low surface coverage most molecules just stay in the monolayer. In order to investigate the influence of the tail region on HB, we further divided the monolayer into primary ($z < 0.4$ nm; $\rho > 30$ M in Fig. 1) and tail ($z > 0.4$ nm; $\rho < 30$ M in Fig. 1) regions. In Fig. 4(b), we computed the contribution to n_{HB} from intramonolayer HB (two-dimensional HB) and from monolayer tail (three-dimensional HB). The contribution from the tail region increases significantly beyond Γ_{crit} while it does not change for $\Gamma < \Gamma_{\text{crit}}$. This implies that the tail region, even though it looks trivial in the density plot, adds three-dimensional HB features and makes the entire HB network more rigid and causes lower diffusion.

To conclude, the lateral diffusion of water on a weak hydrophilic surface exhibits a Λ-shape anomaly. This is in contrast to the critical slowing of water diffusion (V shape) observed in carbon nanotubes.[12] The anomalous behavior can be explained by the normalized molecular free volume. The significant increase in three-dimensional HB from the tail region of the monolayer also contributes to the lower diffusion near full surface coverage.

This research was supported by NSF under Grant Nos. 0120978, 0325344, 0328162, and 0523435 and by NIH under Grant No. PHS 2 PN2 EY016570B.

[1] K. Salaita, Y. Wang, and C. A. Mirkin, Nat. Nanotechnol. **2**, 145 (2007); T. Kraus, L. Malaquin, H. Schmid, W. Riess, N. D. Spencer, and H. Wolf, *ibid.* **2**, 570 (2007); J. Z. Wang, Z. H. Zheng, H. W. Li, W. T. S. Huck, and H. Sirringhaus, Nature Mater. **3**, 171 (2004).
[2] J. H. Park and N. R. Aluru, Chem. Phys. Lett. **447**, 310 (2007); J. Zhao and S. Granick, J. Am. Chem. Soc. **126**, 6242 (2004).
[3] H. J. C. Berendsen, J. R. Grigera, and T. P. Staatsma, J. Phys. Chem. **91**, 6269 (1987).
[4] T. Halicioυğlu and G. M. Pound, Phys. Status Solidi A **30**, 619 (1975).
[5] E. Lindahl, B. Hess, and D. van der Spoel, J. Mol. Model. **7**, 306 (2001).
[6] H. Ö. Pamuk and T. Halicioυğlu, Phys. Status Solidi A **37**, 695 (1976).
[7] S. Nosé, Mol. Phys. **52**, 255 (1984).
[8] J. Hoshen and R. Kopelman, Phys. Rev. B **14**, 3438 (1976).
[9] B. J. Alder and T. Einwohner, J. Chem. Phys. **43**, 3399 (1965).
[10] J. H. Dymond, J. Chem. Phys. **60**, 969 (1974).
[11] A. Luzar and D. Chandler, Nature (London) **379**, 55 (1996).
[12] R. J. Mashl, S. Joseph, N. R. Aluru, and E. Jakobsson, Nano Lett. **3**, 589 (2003).
[13] W. Humphrey, A. Dalke, and K. Schulten, J. Mol. Graphics **14**, 33 (1996).